The Sense of Surface Orientation - A New Sensor Modality for Humanoid Robots

Lukas Kaul, Simon Ottenhaus, Pascal Weiner and Tamim Asfour

***Abstract*— This paper introduces a novel sensor concept for surface exploration in robotic applications. We present an IMU-based haptic sensor that accurately estimates the orientation of contact points. One of the biggest advantages of our proposed sensor concept is the extraction of absolute surface orientation without being affected by inaccuracies in the forward kinematics. Conventional sensors require additional steps to compute surface normals, whereas the proposed concept directly generates normals on contact, leading to accurate surface reconstruction. The introduced sensor is based on off-the-shelf components and costs much less than conventional tactile sensors. We attached our sensor to a 4-DOF robotic arm and conducted several experiments with different objects. Experimental results show that the sense of surface orientation significantly improves surface reconstruction of unknown objects with a method based on Gaussian Implicit Surfaces (GPIS), that is also presented in detail.**

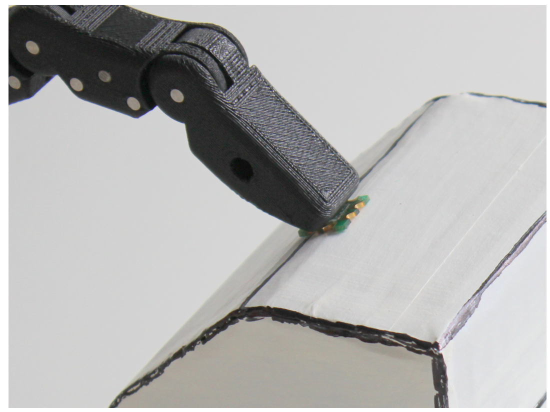

Fig. 1: Exemplification of the basic sensor concept: A robotic finger equipped with a flexibly mounted orientation sensor PCB at its tip.

I. INTRODUCTION

Robots have evolved from industrial machines that merely perform repetitive tasks in fenced-off sections of large-scale factories to very versatile tools. The eventual goal of this development is to create collaborative robots that can safely and intelligently interact with their human counterparts. Making those robots intuitive to interact with and capable of working in human-centered environments are the driving motivations to embody them as humanoid robots.

There are two major challenges that have prevented the vision of collaborative robots to come true yet: The need for light, reliable and affordable torque-controlled robots, as well as the lack of a multimodal perception system that allows safe and intuitive interaction with such robots. Both of these challenges are very active research fields and have seen impressive progress over the recent years.

Addressing the first challenge, torque-controlled robotic arms (e.g. [1]) and even full size humanoid robots such as the ARMAR-4 [2] or the DLR's TORO [3] have been developed. Torque sensing that enables collision detection and interactive teaching of motion are state of the art, even for commercially available robots.

Mimicing the human sensory system appears to be a more difficult challenge, in particular the astonishing haptic capabilities that humans use to enhance their manipulation skills. For many tasks where a human would use tactile feedback from its hands, e.g. assessing the properties and geometry of a visually occluded object, robots typically rely on their vision system. This can be a major drawback when vision is not a feasible option or when the need for a vision system makes the robot's behavior inefficient and not intuitive for the person it interacts with. An example for the difference between humans and most current robots is the way of picking up an unknown object: To be able to successfully grasp the object, the agent must first gain an understanding of the object's geometry. A human would not only use vision and abstraction from prior knowledge, but also haptic feedback from the skin of the fingers, whereas a robot typically relies solely on 'seeing' the object from different angles to understand its geometry.

Reconstructing geometry from tactile feedback is a very challenging task for a robot, in particular due to the fact that the number of samples that it can acquire in a reasonable amount of time is typically very low. There exist a number of sophisticated tactile sensors for humanoid robots [4], [5], [6], that can be used to detect physical contact. An extensive body of work on perceiving object geometry with simple sensors has been established, e.g. by Jentoft et al. in [7] where they deduce object shape from the deformation of compliant finger joints. Some sensors like the one described by Kolker et al. [8] can additionally sense the direction of the contact force, which can potentially improve surface reconstruction. The drawback with this particular sensor, that features an optical system, is its size that effectively prohibits integration into a humanoid fingertip.

Surface reconstruction algorithms can greatly benefit from surface orientation information when contact with an ob-

The research leading to these results has received funding from the European Union's Horizon 2020 Research and Innovation Programme under grant agrement 643950 (SecondHands).

The authors are with the High Performance Humanoid Technologies Lab, Institute for Anthropomatics and Robotics, Karlsruhe Institute of Technology (KIT), Germany, {lukas.kaul, simon.ottenhaus, asfour}@kit.edu

ject is established. This is where the here presented work contributes with a novel idea for a haptic sensor that can provide the orientation of the surface from only one single contact sample. The core of the concept is a small, flexibly mounted MEMS-based orientation sensor on the finger tip that automatically aligns with the contacted surface.

In addition to introducing this new sensor modality we present a proof-of-concept implementation of such a system in Section II, and conduct a number of tests showcasing the benefits this sensor has for reconstructing a haptically explored object shape in Section III. Moreover, we present how our implementation of the sensor can be used for other tasks such as contact detection in Section IV. Section V concludes the paper with a discussion of the obtained results and ideas for further work that can extend this line of research.

II. IMPLEMENTATION

Our proof-of-concept implementation consists of a small orientation sensor connected to the tip of a robotic end-effector with a coil spring that combines the flexibility of a universal joint with an intrinsic restoring force. The sensor is a very small consumer-grade inertial measurement unit (IMU) with on-board data fusion mounted on a custom made breakout board (Fig. 2) including the Bosch BNO055.

A. Sensor

Today's consumer electronics industry's high demand for MEMS-based inertial measurement units for use in smart phones, wearable devices, virtual reality equipment and entertainment products has led to the development of very capable and affordable inertial sensors in increasingly small packages [9]. Moreover, some of these devices feature embedded sensor fusion algorithms for on-board interpreting and refining the raw sensory information into reliable orientation estimates.

One of the smallest and most capable MEMS-based orientation sensors as of today is the Bosch BNO055, a nine axis absolute orientation sensor featuring a triaxial accelerometer, a triaxial gyroscope, a triaxial geomagnetic sensor and a 32-bit ARM cortex M0+ microcontroller running the company's proprietary BSX3.0 FusionLib software. The controller automatically calibrates all sensors and directly computes the absolute orientation from the raw sensor data [10]. The chip is available in a 28 lead LGA package measuring only 3.8 x 5.2 mm^2 with a height of 1.13 mm and can be connected to peripherals via its $\mathrm{I}^2\mathrm{C}$ or UART interfaces. With a price of less than €10 per chip, the BNO055 is well suited for low-cost robotics and bench testing.

B. Sensor Attachment

The key feature of the sensor attachment, that enables surface orientation detection, is the ability to self-align the sensor with the contacted surface. An illustration of this concept can be seen in Fig. 1. As both the surface and the hand orientation can be arbitrary, the joint between the finger tip and the sensor that aligns with the surface needs to allow

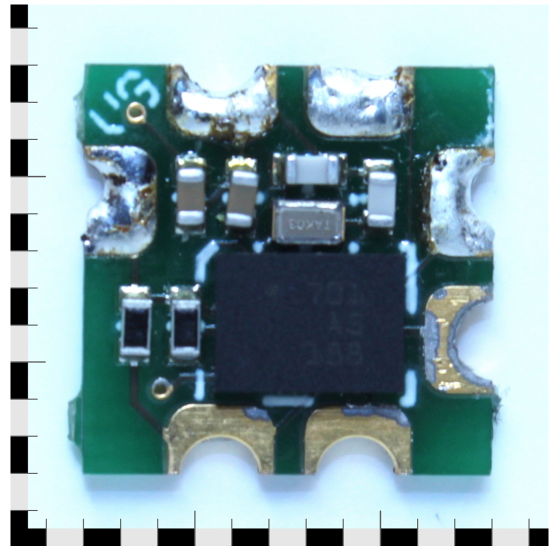

Fig. 2: Our custom breakout board for the Bosch BNO055 and its necessary peripherals. One scale segment equals 1 mm. Note that significantly smaller implementations are possible.

rotations around two axes, i.e. the axes perpendicular to the direction in which the finger tip is pointing. Additionally, a restoring force that orients the sensor back into the initial position relative to the finger tip is needed for repeatable experiments.

Different implementations of such a joint are imaginable: One possiblity is a two-axes gimbal, connecting the finger and the sensor while providing the two necessary rotational degrees of freedom. The drawback of a gimbal is its mechanical complexity and its fragility when manufactured on a scale small enough for the proposed sensor. Another option is a ball joint. However, such a joint provides one rotational degree of freedom too many (around the direction in which the finger is pointing). While this is no problem in principle since the inertial sensor measures absolute orientation and can account for any given rotation, it may cause problems with twisting cables.

Our implementation relies on a coil spring that provides the necessary degrees of freedom through its ability to bend, while intrinsically generating a restoring force to its neutral position without the need for any additional components.

C. Test bed

To realize a proof-of-concept experiment we assembled a planar 4-DOF robotic arm with the spring-mounted sensor attached to the last link (see Fig. 3). The low number of DOF helps to minimize the positional forward kinematics error. The joints of the robot are made of off-the-shelve servo motors with CAN-bus interface (Robotis Dynamixel CX-28) that allow both movement of the end-effector as well as sufficiently precise position measurement. The servos are connected to a PC via a USB/CAN adapter. The BNO055 is connected to an Arduino Due microcontroller [11] over its $\mathrm{I}^2\mathrm{C}$ interface. For the interface, we use the open-source Adafruit BNO055 library [12] and its dependencies. The Arduino Due is connected to the PC over a serial interface.

Fig. 3: The planar 4-DOF robotic arm that we use as test bed. The proposed surface orientation sensor is attached to the tip of the last link with a coil spring.

D. Reconstruction Algorithm

As contact information gathered from tactile exploration can be suspect to noise and forward kinematics errors, a robust reconstruction algorithm is desired. Implicit surfaces are a promising approach to model noisy and sparse data. In the following, we will briefly revisit implicit surfaces and introduce the concept of *Gaussian Processes Implicit Surfaces (GPIS)* and its extension to include normal information.

An implicit surface is defined by its *implicit shape potential (ISP)*. The ISP is typically given by a function

$$f(x) : \mathbb{R}^3 \to \mathbb{R} \begin{cases} = 0, & x \text{ on the surface} \\ > 0, & x \text{ outside} \\ < 0, & x \text{ inside} \end{cases} . \quad (1)$$

This function f can be evaluated at any point x in space and tells if x is inside, outside or exactly on the surface of the estimated object. The estimated surface S is the set of points for which f evaluates to 0:

$$S = \{x, f(x) = 0\} . \quad (2)$$

In the context of tactile and haptic exploration, GPIS are often used to estimate the shape of unknown objects [13], [14], [15], [16]. Williams et. al [17] introduce a special kernel function optimized for implicit surface estimation. For the 3D space, this kernel is defined as

$$k(u, v) = 2\|u - v\|^3 + 2R\|u - v\|^2 + R , \quad (3)$$

where R is the largest distance between any two sample points. The ISP is defined as

$$f(x) = {k_*}^T (K + \sigma^2 \mathbf{I})^{-1} y . \quad (4)$$

The covariance matrix K is calculated using the kernel function k:

$$K_{i,j} = k(x_i, x_j) . \quad (5)$$

The covariance vector k_* is acquired by applying the kernel function k to the test point x and the sample points x_i:

$$k_{*,i} = (x, x_i) . \quad (6)$$

For our setup we need to extend the GPIS approach to include normal information at the observed contact points. To this end the covariance k between two sample points as well as the covariances between the derivatives of k are used during the construction of the covariance matrix K [18, p. 191].

This extension results in the following covariances between two function values, a function value and a partial derivative, and between two partial derivatives:

$$\mathrm{cov}(f_i, f_j) = k(x_i, x_j) \quad (7)$$

$$\mathrm{cov}(f_i, \frac{\partial f_j}{\partial x_{d_j}}) = \frac{\partial k(x_i, x_j)}{\partial x_{d_j}} \quad (8)$$

$$\mathrm{cov}(\frac{\partial f_i}{\partial x_{d_i}}, \frac{\partial f_j}{\partial x_{e_j}}) = \frac{\partial^2 k(x_i, x_j)}{\partial x_{d_i} \partial x_{e_j}} . \quad (9)$$

The covariance matrix K is extended to accommodate all combinations of function values and partial derivatives:

$$K = \begin{bmatrix} k(u,v) & \frac{\partial k(u,v)}{\partial u_1} & \frac{\partial k(u,v)}{\partial u_2} & \frac{\partial k(u,v)}{\partial u_3} \\ & \frac{\partial^2 k(u,v)}{\partial u_1 \partial v_1} & \frac{\partial^2 k(u,v)}{\partial u_1 \partial v_2} & \frac{\partial^2 k(u,v)}{\partial u_1 \partial v_3} \\ & & \frac{\partial^2 k(u,v)}{\partial u_2 \partial v_2} & \frac{\partial^2 k(u,v)}{\partial u_2 \partial v_3} \\ & & & \frac{\partial^2 k(u,v)}{\partial u_3 \partial v_3} \end{bmatrix} \quad (10)$$

Since the covariance matrix K is symmetrical, we only give the upper triangle.

When calculating the necessary partial derivatives of k, three cases have to be distinguished. For simplicity reasons only the partial derivatives for the first two dimensions are provided below. All other derivatives can be calculated by adjusting the indices respectively. The first case is the partial derivative of k in one dimension, needed in Equation 8:

$$\frac{\partial k(u, v)}{\partial u_1} = 6(u_1 - v_1)(R + \|u - v\|) . \quad (11)$$

The second case arises when calculating the covariance defined in Equation 7 for two partial derivatives in the same dimension:

$$\frac{\partial^2 k(u, v)}{\partial u_1 \partial v_1} = 6(R + \|u - v\|) + \frac{6(u_1 - v_1)}{\|u - v\|} . \quad (12)$$

Lastly the covariance between two partial derivatives of k in different dimensions is calculated:

$$\frac{\partial^2 k(u, v)}{\partial u_1 \partial v_2} = \frac{6(u_1 - v_1)(u_2 - v_2)}{\|u - v\|} . \quad (13)$$

Building on this extended definition of GPIS we can introduce derivative information provided by the orientation. To this end, the right side y of the equation system is extended accordingly:

$$y^* = (y_1, n_{1,1}, n_{1,2}, n_{1,3}, y_2, n_{2,1}, n_{2,2}, n_{2,3}, \dots)^T . \quad (14)$$

All observed contact points are comprised of a position and a corresponding surface normal vector (x_i, n_i). Since a contact is only observed on the surface of the object the function values y_i are all 0 by definition of the ISP. The normals

n_i are normalized and correspond to the local gradient of the ISP. The original formulation of GPIS without normal information needs additional points inside and outside of the object to define the potential [17]. This is not necessary for the extended formulation of GPIS, since inside and outside is already defined by the normals and the respective gradient of the ISP. Therefore, no initial assumptions about the object, like size or rough shape, have to be made.

III. EVALUATION

This section presents an evaluation of shape reconstruction based on tactile exploration with the proposed sensor setup, using the hardware described in Section II. The inertial sensor is used to measure the orientation of the surface while the position of the contact point is obtained from the joint angles of the arm and model-based forward kinematics. We use the implicit surface formulation and the *Gaussian Processes Implicit Surfaces* approach for surface reconstruction. We show the difference in performance of the surface reconstruction algorithm when used with and without surface normal information.

A. Experimental Setup

The experimental setup consists of the hardware test bed described in Section II and two different objects to be explored. The arm's end effector is moved to a number of points on the objects until the orientation sensor makes contact and aligns with the surface. The position of the end effector and the measured surface orientation are both recorded for each contact point.

The objects are specifically designed for our evaluation purposes. The fist object ('Stairs') is modeled after a set of stairs with varying step heights. The top is a flat surface, and the side opposing the stairs consists of one angled and one vertical surface (see Fig. 4).

The second object ('Halfpipe') is a box with a semi-circular concave dent in the top side. The outermost parts of the top are horizontal planes, and the sides of the box are vertical.

B. Results

We sampled 15 contact points and their respective surface normals on the Stairs object and 13 on the Halfpipe object. Fig. 4 shows the exploration process and the reconstructed Stairs shape while Fig. 5 shows the Halfpipe and its surface reconstructions. The contribution of the presented work lies in the difference between the reconstruction results with and without taking the surface normal orientation into account, as this is only available through the newly proposed sensor arrangement.

GPIS reconstruction *without the orientation* does not represent the actual shapes very well, see Fig. 4 b) and 5 b). The reconstruction of the stair step geometry is suffering from GPIS's tendency to smooth out edges, while the sparse sampling density of the Halfpipe experiment leads to poor reconstruction results. In contrast, the shape of both the Stairs and especially the sparsely sampled Halfpipe is much better approximated *with the measured surface orientations* taken into account, see Fig. 4 c) and 5 c).

Finally, Figs. 4 d) and 5 d) overlay images of the actual object with their respective shape reconstruction results, emphasizing the improved quality of the shape reconstructions. As can bee seen in the figures, the normal information of the contacts has a high correlation with the actual object surface. However the positional information of the contacts is subject to noise introduced by errors in the forward kinematics. Additionally during the alignment process of the IMU the spring bends and the position of the sensor shifts. This also introduced further errors that are most obvious in Fig. 4 d) resulting in curvatures of originally flat surfaces on the top of the stair steps.

IV. OTHER APPLICATIONS

Other possible applications for the described sensor range from contact detection to robot-human interaction by tapping or moving the sensor to measuring the vibration of contacted objects. In the scope of this paper, we want to briefly show initial results for contact detection.

A. Contact Detection

For tactile exploration of objects, it is crucial to know whether and when contact was made or broken. When the end-effector comes into contact with an object while moving, it will slow down rapidly due to the impact. This leads to a linear acceleration that can be measured with our sensor. As the sensor is extremely light-weight and consequently does not have much inertia, the stopping acceleration is high even at low pre-contact speeds and on soft surfaces. The green and slightly noisy curve in Fig. 6 shows the gravity-compensated absolute linear acceleration during an experiment in which the robot arm repeatedly made contact with a hard surface. The impacts cause very distinct spikes in the acceleration signal that can be detected by simply thresholding the signal. Similarly distinct patterns can be observed in the orientation signal that rapidly deviates from its neutral position as soon as the sensor comes into contact with the surface (see the blue, smooth curve in Fig. 6).

V. CONCLUSION

We proposed the use of a state-of-the-art, highly integrated orientation sensor mounted to the end-effector of a robotic arm in order to measure the orientation of a contacted surface. The orientation sensing is facilitated by the flexible connection between the sensor and the robotic fingertip. The evaluation of the proposed sensor concept in two experiments showed that leveraging directly measured surface orientation can notably improve surface estimation quality, compared to surfaces that are estimated based on contact positions only. The small footprint and simple mounting arrangement of the sensor allows for possible augmentation of existing robotic fingers. Additional measures to ensure that the sensor does not deteriorate the functionality of a grasper would have to be taken, e.g. the spring could be replaced by a smaller implementation of the necessary joint, and the contact-side of the IMU board could be coated with rubber (similar to what

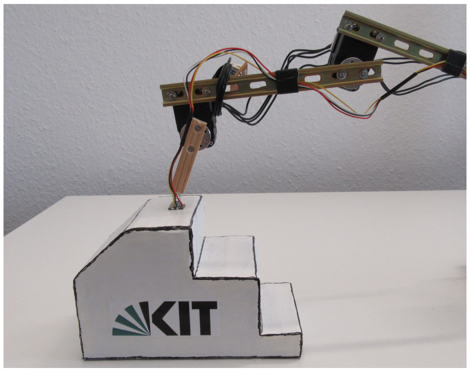

(a) Robotic arm exploring the ’Stairs’ test object

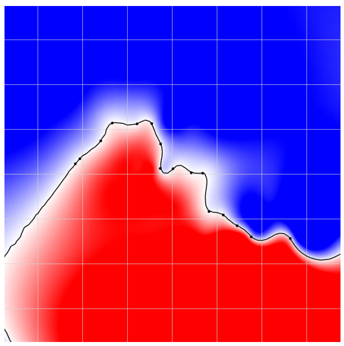

(b) GPIS reconstruction **without** surface normal information

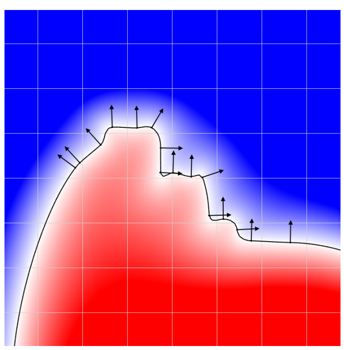

(c) GPIS reconstruction **with** surface normal information

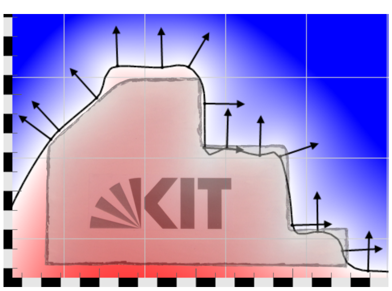

(d) Overlay of the actual object and the GPIS reconstruction with surface normal information. One scale segment equals 1 cm.

Fig. 4: The ’Stairs’ object being explored by the robotic arm and surface reconstructions with and without surface orientation taken into account.

(a) Image of the ’Halfpipipe’ object

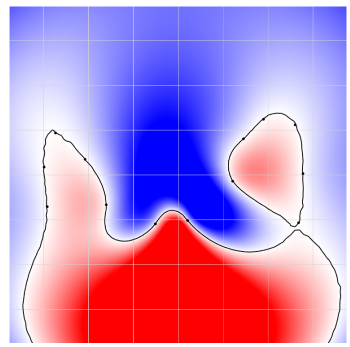

(b) GPIS reconstruction **without** surface normal information

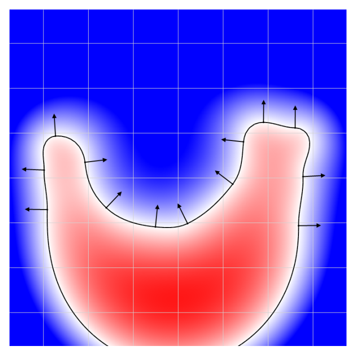

(c) GPIS reconstruction **with** surface normal information

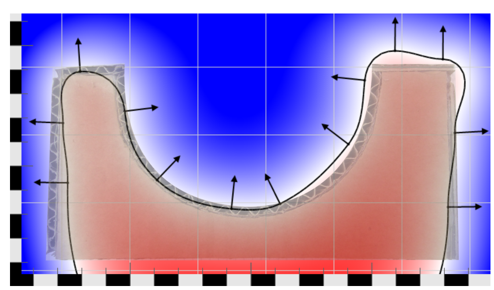

(d) Overlay of the actual object and the GPIS reconstruction with surface normal information. One scale segment equals 1 cm.

Fig. 5: The ’Halfpipe’ object and its reconstructions with and without surface orientation taken into account.

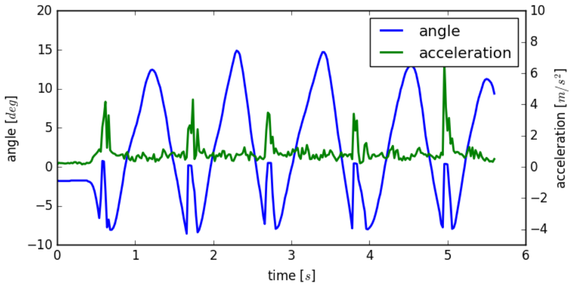

Fig. 6: Angle and absolute acceleration data when touching a surface. The instants of making and breaking contact are distinct in both channels.

has been done in [19]). We also presented an experiment in which the rich IMU data is used to estimate contact events based on distinct changes in acceleration and orientation.

A. *Discussion and Future Work*

This work is intended to present the initial concept and to show its capabilities in a proof-of-concept implementation. In our evaluation, the new sensor proved its capabilities that can be the grounds of innovative further research in the area of haptic exploration. While the spring based construction has its advantages in terms of mechanical simplicity and robustness, it also has certain disadvantages: Most notably, the exact position of the sensor is not known, as the deformation of the spring is not measured. The sensor position is only modeled for the case of an undeformed spring by means of model-based forward kinematics. Lateral deviations from this position are unknown and inevitably lead to small errors in the reconstruction of the examined object shape. Future work could address the modeling of lateral deviations based on the finger's forward kinematics, the measured sensor orientation and the spring characteristics. Secondly, the presented setup is rather large for integration into the finger tip of a human sized robotic hand. This is owed to the fact that the presented construction is a proof-of-concept implementation and not optimized for minimum size. It is possible to design a substantially smaller implementation of this system, even with the same sensor.

The planarity of the robot used for evaluation is a significant restriction. However, as the sensor delivers absolute 3D orientation, and the surface reconstruction algorithm that was presented in Section II is designed to work with 6D poses, omitting the planarity restriction is only a matter of using a more capable arm or hand. The extension to 3D space and objects will be addressed in future work, including the use on one of our humanoid robots (e.g. ARMAR-III [20] or ARMAR-IV [2]).

The presented surface estimation based on Gaussian Processes Implicit Surfaces shows that the explored objects can be reconstructed accurately, as can be seen in Figs. 4 and 5. We are currently working on algorithms aiming to improve the ability to estimate sharp edges and corners of unknown objects over GPIS-approaches, based on multiple contact points with associated normals. Other possible applications like slip detection based on vibration measurement or human-robot interaction in the context of handover tasks are also subject to future work.

References

[1] A. Albu-Schäffer, S. Haddadin, C. Ott, A. Stemmer, T. Wimböck, and G. Hirzinger, "The DLR lightweight robot: Design and control concepts for robots in human environments," *Industrial Robot: An Int. Journal*, vol. 34, no. 5, pp. 376–385, 08 2007.

[2] T. Asfour, J. Schill, H. Peters, C. Klas, J. Bucker, C. Sander, S. Schulz, A. Kargov, T. Werner, and V. Bartenbach, "ARMAR-4: A 63 DOF torque controlled humanoid robot," in *IEEE-RAS Int. Conf. on Humanoid Robots (Humanoids)*, 2013, pp. 390–396.

[3] J. Englsberger, A. Werner, C. Ott, B. Henze, M. A. Roa, G. Garofalo, R. Burger, A. Beyer, O. Eiberger, K. Schmid, and A. Albu-Schäffer, "Overview of the torque-controlled humanoid robot TORO," in *IEEE-RAS Int. Conf. on Humanoid Robots*, 2015, pp. 916–923.

[4] *The BioTac*, SyncTouch, July 2016. [Online]. Available: http://www.syntouchllc.com/Products/BioTac

[5] *TakkStrip*, TakkTile, July 2016. [Online]. Available: http://www.takktile.com/product:takkstrip

[6] G. H. Büscher, R. Koiva, C. Schrmann, R. Haschke, and H. J. Ritter, "Flexible and stretchable fabric-based tactiles sensor," *Robotics and Autonomous Systems*, vol. 63, pp. 244–252, 2015.

[7] L. P. Jentoft and R. D. Howe, "Determining Object Geometry with Compliance and Simple Sensors," in *IEEE/RSJ Int. Conf. on Intelligent Robots and Systems (IROS)*, 2011, pp. 3468–3473.

[8] A. Kolker, M. Jokesch, and U. Thomas, "An Optical Tactile Sensor for Measuring Force Values and Directions for Several Soft and Rigid Contacts," in *Int. Symposium on Robotics (ISR)*, 2016, pp. 63–68.

[9] R. Bogue, "Recent developments in MEMS sensors: a review of applications, markets and technologies," *Sensor Review*, vol. 33, no. 4, pp. 300–304, 2013.

[10] *BNO055 - Intelligent 9-axis absolute orientation sensor*, Bosch Sensortec, June 2016, rev. 1.4. [Online]. Available: https://ae-bst.resource.bosch.com/media/_tech/media/datasheets/BST_BNO055_DS000_14.pdf

[11] *Arduino Due*, arduino.cc, July 2016. [Online]. Available: https://www.arduino.cc/en/Main/ArduinoBoardDue

[12] *Adafruit Unified BNO055 Driver (AHRS/Orientation)*, Adafruit, July 2016. [Online]. Available: https://github.com/adafruit/Adafruit_BNO055

[13] S. Dragiev, M. Toussaint, and M. Gienger, "Gaussian process implicit surfaces for shape estimation and grasping," in *IEEE Int. Conf. on Robotics and Automation (ICRA)*, 2011, pp. 2845–2850.

[14] N. Sommer, M. Li, and A. Billard, "Bimanual compliant tactile exploration for grasping unknown objects," in *IEEE Int. Conf. on Robotics and Automation (ICRA)*, 2014, pp. 6400–6407.

[15] M. Bjorkman, Y. Bekiroglu, V. Hogman, and D. Kragic, "Enhancing visual perception of shape through tactile glances," in *IEEE/RSJ Int. Conf. on Intelligent Robots and Systems (IROS)*, 2013, pp. 3180–3186.

[16] M. G. López, B. Mederos, and O. Dalmau, "Gp-mpu method for implicit surface reconstruction," in *Human-Inspired Computing and Its Applications*. Springer, 2014, pp. 269–280.

[17] O. Williams and A. Fitzgibbon, "Gaussian process implicit surfaces," *Gaussian Proc. in Practice*, 2007.

[18] C. E. Rasmussen and C. Williams, *Gaussian processes for machine learning*. MIT Press, 2006.

[19] Y. Tenzer, L. P. Jentoft, and R. D. Howe, "The Feel of MEMS Barometers: Inexpensive and Easily Customized Tactile Array Sensors," *IEEE Robotics Automation Magazine*, vol. 21, no. 3, pp. 89–95, Sept 2014.

[20] T. Asfour, K. Regenstein, P. Azad, J. Schroder, A. Bierbaum, N. Vahrenkamp, and R. Dillmann, "ARMAR-III: An integrated humanoid platform for sensory-motor control," in *IEEE-RAS Int. Conf. on Humanoid Robots (Humanoids)*, 2006, pp. 169–175.